ELSEVIER

Pattern Recognition Letters 23 (2002) 1687–1693

Pattern Recognition Letters

www.elsevier.com/locate/patrec

Fast and robust recognition of orbit and sinus drawings using histograms of forces

Laurent Wendling [a], Salvatore Tabbone [a,*], Pascal Matsakis [b]

[a] *LORIA-UMR 7503, Campus Scientifique, BP 239, 54506 Vandoeuvre-les-Nancy Cedex, France*
[b] *CECS Department, University of Missouri-Columbia, Columbia, MO 65211, USA*

Received 14 July 2000; received in revised form 21 December 2001

Abstract

The notion of the histogram of forces was introduced in a previous work with the aim of modeling spatial relations between image objects. In this paper, we show that it can also be useful in pattern recognition. Drawings of cranial orbits and sinuses are classified using force histograms. The results are consistent with human responses, and our method compares favorably with classical methods based on geometric criteria and Fourier descriptors.

Keywords: Force histograms; *F*-signatures; Pattern recognition; Shape matching

1. Introduction

The database used in this study is composed of several orbit and sinus drawings provided by a French medicine team (University Paul Sabatier of Toulouse France). These drawings were defined from craniums (3rd century AD) found in a necropolis (Nubia Vila, 1994). Experts (Szilvassy, 1982) distinguish four models of sinuses (bean, foliaceous, pyramidal, fan-shaped) and four models of orbits (rectangular, elliptical, trapezoid, circular). Each drawing is composed of two orbits and two sinuses. The two orbits belong to the same class whereas the two sinuses are independent. Our aim is to classify each orbit and sinus of the database using the notion of the histogram of forces (Matsakis, 1998; Matsakis and Wendling, 1999). For each drawing, three histograms are computed. They represent the position (i) of the right orbit relative to the left one, (ii) of the right sinus relative to itself, (iii) of the left sinus relative to itself. The three histograms are then matched against histograms computed from prototypes. To validate our approach, we have conducted a blind test with one hundred people. Each person was asked to classify each sinus and each pair of orbits according to the prototypes. Moreover, we have conducted a comparative study with classical methods based on geometric features and Fourier descriptors.

The use of geometric features is discussed in Section 2. The notion of the histogram of forces is briefly reviewed in Section 3. The force

* Corresponding author. Tel.: +33-8359-2000; fax: +33-8341-3079.
E-mail address: tabbone@loria.fr (S. Tabbone).

0167-8655/02/$ - see front matter
PII: S0167-8655(02)00131-9

histogram-based method of classifying orbit and sinus drawings is described in Section 4. Experimental results are presented in the same section. Conclusion is given in Section 5.

2. Shape classification using geometric features

In first experiments (Matsakis and Wendling, 2000), two classical geometric features were used to classify the orbit and sinus drawings: the degree of compactness and the degree of ellipticity (the axes being given by the moments of order 0–2 (Teag, 1980)). These features and their combination yielded poor results. For instance, since the perimeter has a strong effect on the calculation of the compactness, orbits and sinuses are often misclassified when the drawings are not sharp. Furthermore, it is a well-known fact that approaches based on feature descriptors are sensitive to noise and occlusions (Belkasim et al., 1991; Ghorbel, 1994; Lin and Shen, 1991; Zhan and Roskies, 1972).

A polygonal approximation of the objects could be a solution to this problem. However, it induces loss of information, which may result in lower recognition rates. The degree of ellipticity is not suited either to the classification of this type of object. Maes (1991), for example, presented a string-matching technique for recognizing and classifying polygons; but the strength of this method is limited when the polygonal approximation of the object is inconsistent. Gerdes et al. (1995) proposed another approach based on contour-oriented 2D object recognition, which is less sensitive to polygonal approximation inconsistency. Its main drawback is its time complexity, especially when many models have to be identified. The generalized Hough transform Ballard, 1981 is also a useful technique for shape recognition, but its drawbacks—computation time and storage requirements—are substantial. Even though improvements were proposed (Kassim et al., 1999) the approach remains complex when many models have to be characterized. The method presented in this paper is invariant under rotation and scaling. Furthermore, it is of low time complexity, and is able to handle non polygonal objects as well as polygonal objects.

3. The histogram of forces

The notion of the histogram of forces was introduced by Matsakis (1998) and presented by Matsakis and Wendling (1999). It generalizes and supersedes the histogram of angles described by Krishnapuram et al. (1993) and Miyajima and Ralescu (1994). Consider two 2D objects A and B (see Fig. 1). The histogram of forces associated with these objects is a quantitative representation of their relative position. Let r be any real number and let φ_r be the function from $\mathbb{R}$ into $\mathbb{R}_+$, null on $\mathbb{R}_-$, such that:

$$\forall d \in \mathbb{R}_+^*, \varphi_r(d) = 1/d^r \tag{1}$$

$\varphi_r(d)$ corresponds to the elementary attraction force exerted by one point of A on one point of B. The symbol d denotes the distance between the two points considered, and r characterizes the forces involved. For instance, the forces are constant if r is 0, and are of gravitational type if r is 2.

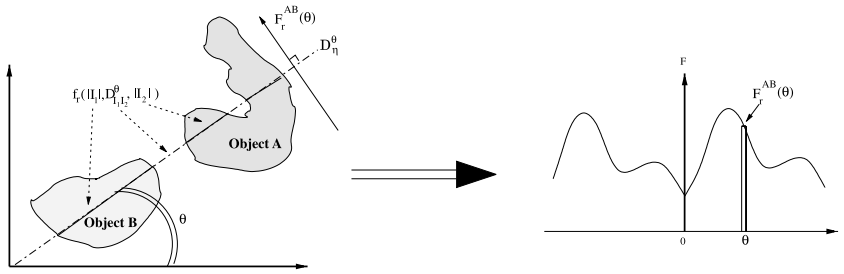

Fig. 1. Force histogram computation.

In practice, to decrease the computation time, attraction forces are computed between aligned segments, not between points. Let I and J be two segments of an oriented straight line that defines with the X-axis an angle θ. These segments are of length $|I|$ and $|J|$, and their relative position on the line is perfectly determined by a real number D^{θ}_{IJ}. The attraction force exerted by I on J is computed as follows:

$$f_r(|I|, D^{\theta}_{IJ}, |J|) = \int_{D^{\theta}_{IJ}+|J|}^{|I|+D^{\theta}_{IJ}+|J|} \int_0^{|J|} \varphi_r(u-v)\,\mathrm{d}v\,\mathrm{d}u \tag{2}$$

For each direction θ, there exists a pencil of parallel lines that describe entirely the objects A and B. Let us consider one particular line, denoted by $\mathscr{D}^{\theta}_{\eta}$. Since A and B are not necessarily convex, $\mathscr{D}^{\theta}_{\eta}$ generally defines two sets of segments: $A_\theta(\eta) = \cup\{I_i\}_{i=1,n}$ and $B_\theta(\eta) = \cup\{J_j\}_{j=1,m}$. The mutual attraction between these sets is:

$$F_r(\theta, A_\theta(\eta), B_\theta(\eta)) = \sum_{i\in 1\ldots n} \sum_{j\in 1\ldots m} f_r(|I_i|, D^{\theta}_{I_iJ_j}, |J_j|) \tag{3}$$

The sum of these forces when η describes the set of real numbers, i.e., when $\mathscr{D}^{\theta}_{\eta}$ describes the considered pencil, is denoted by $F_r^{AB}(\theta)$. It is the scalar resultant of elementary forces: these forces are exerted by the points of A on those of B, and each tends to move B in direction θ. The values $F_r^{AB}(\theta)$ define the F_r-histogram F_r^{AB} associated with the objects A and B. If the two objects are identical, the F_r-histogram is called the F_r-signature of the object. In practice, of course, only a finite number of evenly distributed directions are considered. Force histograms have nice geometric properties, which are exploited in Section 4. For instance:

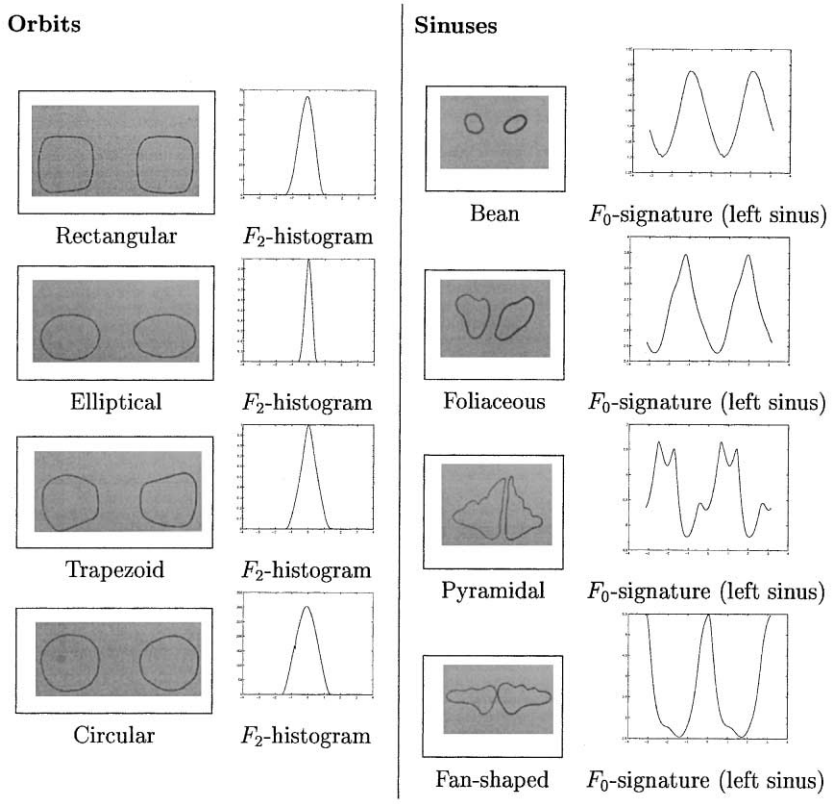

Fig. 2. Prototypes of classes of orbits and sinuses.

- F_r^{BA} can easily be deduced from F_r^{AB},
- when A and B are translated, F_r^{AB} remains the same,
- when a rotation is applied, the histogram is simply shifted along its θ-axis,
- when a dilation (i.e., homothety) is applied, the histogram is stretched (the forces are multiplied by a value that depends on r and on the scale factor).

4. Experiments

4.1. Description

About forty drawings of orbits and sinuses—defined from craniums found in a necropolis—constituted the test database. Each drawing was scanned and for each image, six histograms were computed (histograms of constant forces and

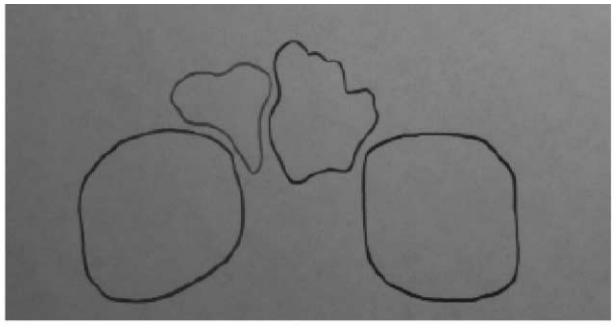

Similarity ratios (F_0)

Orbits		Sinus	left	right
Re	**94.90**	Be	22.05	11.67
El	85.89	Fo	**92.32**	37.90
Tr	89.60	Py	85.62	**80.74**
Ci	93.52	Fs	59.07	38.42

Similarity ratios (normalized F_0-histograms)

Orbits		Sinus	left	right
Re	**96.51**	Be	65.62	39.07
El	79.39	Fo	**92.32**	66.40
Tr	87.88	Py	82.14	**72.90**
Ci	92.53	Fs	56.48	33.63

Similarity ratios (F_2)

Orbits		Sinus	left	right
Re	**97.49**	Be	7.59	1.37
El	82.68	Fo	61.32	11.09
Tr	78.96	Py	**89.68**	**37.33**
Ci	95.30	Fs	57.57	10.41

Similarity ratios (normalized F_2-histograms)

Orbits		Sinus	left	right
Re	**96.51**	Be	59.31	37.29
El	83.00	Fo	**95.20**	62.23
Tr	88.10	Py	90.36	**78.20**
Ci	93.33	Fs	68.99	43.27

Similarity ratios from Fourier descriptors

Orbits		Sinus	left	right
Re	**55.61**	Be	32.26	35.16
El	51.00	Fo	**55.34**	**57.22**
Tr	48.74	Py	40.82	52.25
Ci	40.93	Fs	48.72	44.97

People opinion (%)

Orbits		Sinus	left	right
Re	**69**	Be	0	1
El	3	Fo	**49**	16
Tr	16	Py	8	**79**
Ci	12	Fs	33	4

Fig. 3. First example: image misa_1.

gravitational forces, F_0 and F_2, for the pair of orbits, and for each sinus). The classification of orbits and sinuses is based on the computation of similarities between the histograms associated with the test images and those associated with prototypes provided by experts. Consider two histograms H_1 and H_2. The similarity ratio SR (expressed as a percentage) between H_1 and H_2 is defined as in formula 4, where $\overline{H}_1$ and $\overline{H}_2$ denote the normalized histograms. Hence, SR is not sensitive to object scaling. Moreover, note that circular shifts α are applied to $\overline{H}_2$, and SR is obtained by maximizing the classical Tanimoto index (min over max). In that way, SR is not sensitive to object rotation either.

$$\mathrm{SR}(H_1, H_2) = 100 \max_{\alpha} \left\{ \frac{\sum_{\theta} \min(\overline{H}_1(\theta), \overline{H}_2(\theta+\alpha))}{\sum_{\theta} \max(\overline{H}_1(\theta), \overline{H}_2(\theta+\alpha))} \right\} \quad (4)$$

To assess the accuracy of our approach and its consistency with human perception, we have conducted a blind test with a population of 100 people. Each person was asked to classify the cranial orbits and sinuses according to the prototypes and the fact that in each drawing the two orbits belong to the same class whereas the two sinuses are independent. We also compared our method with a method implemented from Zhan and Roskies (1972) and based on the computation of Fourier descriptors (up to the 15th order).

4.2. Prototypes

See Fig. 2; eight drawings defined by an expert constituted the prototypes of the classes of orbits and sinuses. The two orbits belong to the same class whereas the two sinuses are independent. Each drawing was scanned and the regions corresponding to the orbits and sinuses were

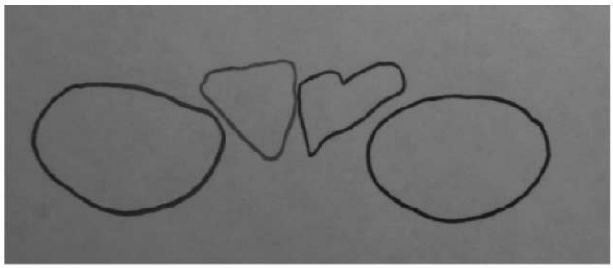

Similarity ratios (normalized F_0-histogram)

Orbits		Sinus	left	right
Re	**62.87**	Be	67.86	**91.13**
El	76.07	Fo	**96.40**	73.30
Tr	68.92	Py	79.43	58.42
Ci	65.75	Fs	58.41	79.32

Similarity ratios (normalized F_2-histogram)

Orbits		Sinus	left	right
Re	53.55	Be	63.31	81.46
El	**74.14**	Fo	**94.29**	81.43
Tr	70.09	Py	84.66	65.79
Ci	66.20	Fs	73.65	**93.57**

Similarity ratios from Fourier descriptors

Orbits		Sinus	left	right
Re	58.49	Be	43.50	32.29
El	**60.06**	Fo	**57.86**	**60.31**
Tr	54.46	Py	38.17	50.06
Ci	35.52	Fs	36.84	45.39

People opinion (%)

Orbits		Sinus	left	right
Re	2	Be	0	0
El	**83**	Fo	**67**	32
Tr	1	Py	22	16
Ci	14	Fs	11	**52**

Fig. 4. Second example: image misa_11.

determined using a classical binarization method. Then 24 histograms were computed. Half are histograms of constant forces (F_0) and half are histograms of gravitational forces (F_2). Each histogram represents the relative position (i) of the right orbit with regard to the left one or (ii) of the right sinus with regard to itself or (iii) of the left sinus with regard to itself (in cases (ii) and (iii), the histograms are F-signatures).

4.3. Representative results

In this section, we examine three representative results. The different classes of orbits and sinuses are denoted by Re (rectangular), El (elliptical), Tr (trapezoid) and Ci (circular) for the orbits; Be (bean), Fo (foliaceous), Py (pyramidal) and Fs (fan-shaped) for the sinuses.

This first example (see Fig. 3) illustrates the fact that if the histograms were not normalized (see Eq. (4)) then numerous misclassifications would be encountered—mostly because the size of the sinuses vary a lot from one cranium to the other. On the other hand, the results obtained with normalized histograms are compatible with the opinion expressed by the majority of people.

Even normalized, the F_0-histograms may lead to incorrect classifications. In this second example (see Fig. 4) the right sinus is actually fan-shaped, and not bean-shaped (according to most people).

The use of normalized F_2-histograms allows most of the orbits and sinuses to be classified correctly, but the method is not foolproof. In the case of this drawing, for instance, the orbits are misclassified (see Fig. 5). It is not clear, however, whether they are circular or trapezoid, and the

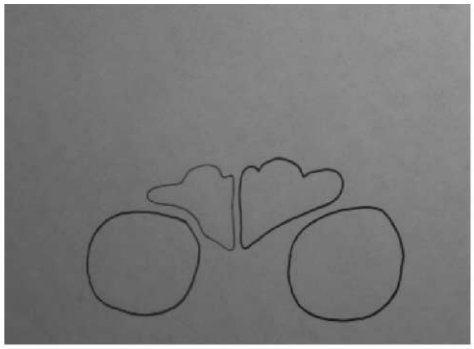

Similarity ratios (normalized F_2-histograms)

Orbits		Sinus	left	right
Re	90.21	Be	51.42	55.82
El	**92.93**	Fo	86.11	93.36
Tr	96.52	Py	**95.87**	**95.67**
Ci	94.14	Fs	59.82	64.94

Similarity ratios from Fourier descriptors

Orbits		Sinus	left	right
Re	51.16	Be	35.83	42.23
El	**61.05**	Fo	**54.16**	**61.77**
Tr	49.46	Py	34.89	49.34
Ci	45.78	Fs	42.02	63.17

People opinion (%)

Orbits		Sinus	left	right
Re	13	Be	0	0
El	11	Fo	28	31
Tr	37	Py	**57**	**53**
Ci	**39**	Fs	15	16

Fig. 5. Third example: image misa_8.

people are divided. There are three ambiguous cases like this one in the whole database.

Finally, note that the method based on the computation of Fourier descriptors yields poor results. It is often unable to distinguish between the different orbit classes, and the sinuses are generally assigned to the same class (foliaceous).

The complexity of the presented approach is in $\mathcal{O}(pn\sqrt{n})$ where n denotes the number of pixels of the processed image and p the number of directions in which forces are computed. It drops to $\mathcal{O}(pn)$ for convex objects. The experiments were carried out with $p = 128$. When using a greater value, the similarity ratios differ by 0.1% only.

5. Conclusion

We have shown in this paper that the notion of the histogram of forces (Matsakis, 1998; Matsakis and Wendling, 1999) can be exploited in pattern recognition. In particular, the F-signature (Matsakis, 1998; Matsakis and Wendling, 2000) of an image region proves to be a powerful representation of its shape. The use of force histograms allows shapes to be categorized consistently with human perception. Compared to classical methods based on geometric features or Fourier descriptors, the histogram-based method presented in this paper is of lower computing time and leads to much higher classification accuracy.

References

Ballard, D.H., 1981. Generalizing the Hough transform to detect arbitrary shapes. Pattern Recognition 13 (2), 111–122.

Belkasim, S.O., Shridar, M., Ahmadi, M., 1991. Pattern recognition with moment invariants: a comparative study and new results. Pattern Recognition 24, 1117–1138.

Gerdes, R., Otterbach, R., Kammuler, R., 1995. Fast and robust recognition and localization of 2D objects. MVA 8, 365–374.

Ghorbel, F., 1994. A complete invariant description for gray level images by analysis approach. PRL 15, 1043–1051.

Kassim, A.A., Tan, T., Tan, K.H., 1999. A comparative study of efficient generalized Hough transform techniques. IVC 17, 737–748.

Krishnapuram, R., Keller, J.M., Ma, Y., 1993. Quantitative analysis of properties and spatial relations of fuzzy image regions. IEEE Transactions on Fuzzy Systems 1 (3), 222–233.

Lin, B.C., Shen, J., 1991. Fast computation of moment invariants. Pattern Recognition 24, 807–813.

Maes, M., 1991. Polygonal shape recognition using string-matching techniques. Pattern Recognition 24 (5), 433–440.

Matsakis, P., 1998. Relations spatiales structurelles et interprétation d'images, Ph.D. Thesis, Institut de Recherche en Informatique de Toulouse, France.

Matsakis, P., Wendling, L., 1999. A new way to represent the relative position between areal objects. IEEE PAMI 21 (7), 634–643.

Matsakis, P., Wendling, L., 2000. Orbit and sinus classification based on force histogram computation. In: Aravind, B. (Ed.), IAPR International Conference on Pattern Recognition, Proceedings, vol. 2, pp. 451–454.

Miyajima, K., Ralescu, A., 1994. Spatial organization in 2D segmented images: representation and recognition of primitive spatial relations. Fuzzy Sets and Systems 65 (2/3), 225–236.

Teag, R., 1980. Image analysis via the general theory of moments. Optical Society of America 70 (8), 920–921.

Szilvassy, J., 1982. Zur Variation Entwicklung und Vererbung der Stirnhohlen. Ann. Naturhist. mus. Wien. 1, 97–125.

Vila, A., 1994. La prospection archéologique de la vallée du Nil au sud de la catarcate de Dal, Editions du CNRS. Paris fasc. 1 á 15, pp. 97–125.

Zhan, C.T., Roskies, R.Z., 1972. Fourier descriptors for plane closed curves. IEEE Transactions on Computers C-21, 269–281.